The MMX Rover: Performing in-situ Surface Investigations on Phobos

Patrick Michel (michelp@oca.eu)
CNRS Délégation Côte d'Azur https://orcid.org/0000-0002-0884-1993
Stephan Ulamec
DLR: Deutsches Zentrum fur Luft- und Raumfahrt
Ute Boettger
DLR
Matthias Grott
DLR Berlin: Deutsches Zentrum fur Luft- und Raumfahrt DLR Standort Berlin
Naomi Murdoch
ISAE-SUPAERO
Pierre Vernazza
LAM: Laboratoire d'Astrophysique de Marseille
Cecily Sunday
ISAE-SUPAERO
Yun Zhang
UCA: Universite Cote d'Azur
Rudy Valette
CEMEF: Centre de mise en forme des materiaux
Romain Castellani
CEMEF: Centre de mise en forme des materiaux
Jens Biele
DLR: Deutsches Zentrum fur Luft- und Raumfahrt
Simon Tardivel
French Space Agency: CNES
Olivier Groussin
LAM: Laboratoire d'Astrophysique de Marseille
Laurent Jorda
LAM: Laboratoire d'Astrophysique de Marseille
Joerg Knollenberg
DLR: Deutsches Zentrum fur Luft- und Raumfahrt
Jan Thimo Grundmann
DLR: Deutsches Zentrum fur Luft- und Raumfahrt
Denis Arrat

French Space Agency: CNES

Gabriel Pont

French Space Agency: CNES

Stéphane Mary

French Space Agency: CNES

Markus Grebenstein

DLR: Deutsches Zentrum fur Luft- und Raumfahrt

Hirdy Miyamoto

University of Tokyo: Tokyo Daigaku

Tomoki Nakamura

Tohoku University Graduate School of Science Faculty of Science: Tohoku Daigaku Daigakuin Rigaku Kenkyuka Rigakubu

Koji Wada

Chiba Institute of Technology: Chiba Kogyo Daigaku

Kent Yoshikawa

JAXA

Kiyoshi Kuramoto

Hokkaido University: Hokkaido Daigaku

Full paper

Keywords: Camera, Numerical Modeling, Phobos, Radiometer, Raman Spectrometer, Regolith, Regolith Dynamics,101 Thermal Inertia, Rover102

Posted Date: January 15th, 2021

DOI: https://doi.org/10.21203/rs.3.rs-139920/v1

The MMX rover: performing in-situ surface investigations on Phobos

Patrick Michel*, Université Côte d'Azur, Observatoire de la Côte d'Azur, CNRS, Laboratoire Lagrange, Nice, 06304, France, michelp@oca.eu

Stephan Ulamec, Deutsches Zentrum für Luft- und Raumfahrt e.V. (DLR), Linder Höhe, Cologne, 51147, Germany, Stephan.Ulamec@dlr.de

Ute Boettger, Deutsches Zentrum für Luft- und Raumfahrt e.V. (DLR), Institute of Optical Sensor Systems, 12489 Berlin, Rutherfordstr. 2, Germany, Ute.Boettger@dlr.de

Matthias Grott, Deutsches Zentrum für Luft- und Raumfahrt e.V. (DLR), Institut für Planetenforschungn Rutherfordstrasse 2, 12489 Berlin, Germany, Matthias.Grott@dlr.de

Naomi Murdoch, ISAE-SUPAERO, Université de Toulouse, DEOS/Space Systems for Planetary Applications, 10 avenue Edouard Belin, BP 54032, 31055 Toulouse Cedex 4, France, Naomi.MURDOCH@isae-supaero.fr

Pierre Vernazza, Aix Marseille Université, CNRS, CNES, Laboratoire d'Astrophysique de Marseille, Marseille, France, pierre.vernazza@lam.fr

Cecily Sunday, Université de Toulouse, DEOS/Space Systems for Planetary Applications, 10 avenue Edouard Belin, BP 54032, 31055 Toulouse Cedex 4, France, Cecily.SUNDAY@isae-supaero.fr

Yun Zhang, Université Côte d'Azur, Observatoire de la Côte d'Azur, CNRS, Laboratoire Lagrange, Nice, 06304, France, yun.zhang@oca.eu

Rudy Valette, Mines ParisTech, PSL Research University, CEMEF, Centre for Material Forming, CNRS UMR 7635, CS 10207 rue Claude Daunesse, 06904 Sophia Antipolis Cedex, France, rudy.valette@mines-paristech.fr

Romain Castellani, Mines ParisTech, PSL Research University, CEMEF, Centre for Material Forming, CNRS UMR 7635, CS 10207 rue Claude Daunesse, 06904 Sophia Antipolis Cedex, France, romain.castellani@mines-paristech.fr

Jens Biele, Deutsches Zentrum für Luft- und Raumfahrt e.V. (DLR), Linder Höhe, Cologne, 51147, Germany, jens.biele@dlr.de

Simon Tardivel, CNES, BPI 2532, Laplace 116B, 18 avenue Édouard Belin, 31401 Toulouse Cedex 9, France, Simon.Tardivel@cnes.fr

Olivier Groussin, Aix Marseille Université, CNRS, CNES, Laboratoire d'Astrophysique de Marseille, Marseille, France, olivier.groussin@lam.fr

Laurent Jorda, Aix Marseille Université, CNRS, CNES, Laboratoire d'Astrophysique de Marseille, Marseille, France, laurent.jorda@lam.fr

Joerg Knollenberg, Deutsches Zentrum für Luft- und Raumfahrt e.V. (DLR), Institut für Planetenforschungn Rutherfordstrasse 2, 12489 Berlin, Germany, Joerg.Knollenberg@dlr.de

Jan Thimo Grundmann, Deutsches Zentrum für Luft- und Raumfahrt e. V. (DLR), Institute of Space Systemsn Robert-Hooke-Strasse 7, D-28359 Bremen, Germany, Jan.Grundmann@dlr.de

Denis Arrat, CNES, BPI 2532, Laplace 116B, 18 avenue Édouard Belin, 31401 Toulouse Cedex 9, France, Denis.Arrat@cnes.fr

Gabriel Pont, CNES, BPI 2532, Laplace 116B, 18 avenue Édouard Belin, 31401 Toulouse Cedex 9, France, Gabriel.Pont@cnes.fr

Stephane Mary, Directorate for Orbital Systems / Science Project Department, 18 avenue Edouard Belin, 31401 Toulouse Cedex 9, France, Stephane.Mary@cnes.fr

Markus Grubestein, Deutsches Zentrum für Luft- und Raumfahrt e.V. (DLR), 82234 Oberpfaffenhofen, Germany, Markus.Grebenstein@dlr.de

Hirdy Miyamoto, Department of Systems Innovation, University of Tokyo, 7-3-1 Hongo, Bunkyo-ku, Tokyo 113-8656, Japan, hm@sys.t.u-tokyo.ac.jp

Tomoki Nakamura, Laboratory for Early Solar System Evolution, Department of Earth Science, Graduate School of Science, Tohoku University, Aoba, Sendai, Miyagi 980-8578, Japan, tomoki.nakamura.a8@tohoku.ac.jp

Koji Wada, Planetary Exploration Research Center (PERC), Chiba Institute of Technology (Chitech), Tsudanuma 2-17-1, Narashino, Chiba 275-0016, Japan, wada@perc.it-chiba.ac.jp

Kent Yoshikawa, Research and Development Directorate, Japan Aerospace Exploration Agency, Sagamihara 252-5210, Japan, yoshikawa.kento@jaxa.jp

Kiyoshi Kuramoto, Faculty of Science, Hokkaido University Kita-10 Nishi-8, Kita-ku, Sapporo 060-0810, JAPAN, keikei@ep.sci.hokudai.ac.jp

Joint first authors: P. Michel and S. Ulamec contributed equally to this work

*Corresponding author: michelp@oca.eu

Preprint submitted to *Earth, Planets and Space* on January 1, 2021

Abstract

The Japanese MMX sample return mission to Phobos by JAXA will carry a Rover developed by CNES and DLR that will be deployed on Phobos to perform in-situ analysis of the Martian moon's surface properties. Past images of the surface of Phobos show that it is covered by a layer of regolith. However, the mechanical and compositional properties of this regolith are poorly constrained. In particular nothing is known regarding the particle sizes, their chemical composition, the packing density of the regolith as well as other frictional parameters and surface dynamics from current remote images. Understanding the properties and dynamics of the regolith in the low-gravity environment of Phobos is important to trace back its history and surface evolution. Moreover, this information is also important to support the interpretation of data obtained by instruments onboard the main spacecraft and to minimize the risks involved in the sampling by the spacecraft. The instruments onboard the Rover are an infrared radiometer (miniRad), a Raman spectrometer (RAX), two cameras looking forwards for navigation and science purposes (NavCams), and two cameras observing the flow of regolith around the rover wheels (WheelCams). The Rover will be deployed before the sampling of Phobos' surface by MMX spacecraft and will be the first rover driving on a Martian moon and in a low-gravity environment.

Keywords

Camera, Numerical Modeling, Phobos, Radiometer, Raman Spectrometer, Regolith, Regolith Dynamics, Thermal Inertia, Rover

Introduction

The MMX Rover is a contribution by the Centre National d'Etudes Spatiales (CNES) and the German Aerospace Center (DLR) to the Martian Moons eXploration (MMX) mission by the Japan Aerospace Agency, JAXA, to the Martian moons Phobos and Deimos (Kuramoto et al. 2017; Kawakatsu et al. 2019). It will be delivered to the surface of Phobos to perform in-situ science but also to serve as a scout, preparing the landing of the main spacecraft. The Rover is planned to be released from the mother spacecraft at an altitude of less than 100 m (the current baseline foresees 45 m), ballistically descend to the surface of Phobos and come to rest in an arbitrary attitude after several bounces. After this it

will upright itself and deploy its solar panels. In addition to its scientific objectives, as described in the following section, the MMX Rover will demonstrate locomotion using on wheels in a low gravity environment. The distance the rover can move on the surface of Phobos will strongly depend on the actual terrain that is not yet known, thus no strict requirements have been set (such as described in, e.g., Lorenz 2020). During the rover mission a total distance from a few meters to hundreds of meters may be covered. All telemetry and commands will be sent via the MMX mother spacecraft, acting as a relay. More details on the rover system are given by Ulamec et al. (2019).

General Science Objectives

The scientific objectives of the MMX rover are defined in line with those of the overall MMX mission, complementing the science which can be performed with the instruments on board the main spacecraft or the returned samples.

These instruments are two navigations cameras (called NavCams), two cameras that will observe the regolith flow on the back and front wheels (called WheelCams), a Raman spectrometer (called RAX) and a miniaturized radiometer (called miniRad). Figure 1 shows the rover deployed configuration and its internal compartment, while Fig. 2 shows its on-surface configuration.

The data provided by the rover instrument suite are extremely valuable for the communities interested in regolith dynamics in the low gravity environment of Phobos, in surface processes, in the formation, geological history and composition of Phobos, and in its thermal properties. The data set that will be obtained in-situ is of high value for the interpretation of data obtained remotely by the spacecraft. It will add ground truth, and provide a geological context to the samples that will be returned to Earth in order to clarify the origin and history of Phobos.

The Rover will perform:

- Close-up and high resolution imaging of the surface terrain.
- Regolith science (e.g. dynamics, mechanical properties like surface strength, cohesion; geometrical properties like grain size distribution, porosity).
- Measurements of the mineralogical composition of the surface material (by Raman spectroscopy).
- Determination of the thermal properties of the surface material (surface temperature, emissivity, thermal conductivity, layering).

The measurements by the MMX rover will allow determination of the heterogeneity of the surface material

and thus will support the MMX landing and sampling. Furthermore, the characterization of the regolith properties shall considerably reduce the risk of the landing (and sampling) of the main spacecraft, as the rover will offer the only direct measurements of Phobos' surface response to an external action.

Science with the Raman Spectrometer (RAX)

In line with the top-level science objectives of the MMX mission as defined by JAXA, namely gaining knowledge about the origin, evolution, and formation of Solar System bodies, Raman spectroscopy will be used to provide in-situ information about Phobos' geochemical composition. For this a Raman spectrometer onboard the rover will investigate its surface mineralogy in the μm scale. This Raman spectrometer for MMX (RAX) (Fig. 3) is a compact, low-mass instrument with a volume of approximately $81 \times 98 \times 125$ mm^3 and a mass of less than 1.4 kg developed by DLR, INTA/UVA and JAXA/UTOPS/Rikkyo (Cho et al. 2020, , this issue). It is designed to withstand the harsh conditions on Phobos and will be the first Raman spectrometer on an airless body. The measurements performed with RAX include the identification of minerals on various points on the surface of Phobos, validated by comparison with experiments in laboratories on Earth and spectral laboratory reference data bases. The acquired data will support and complement the orbiter spectroscopic measurements and the measurements performed on the returned samples as ground truth. Furthermore, the RAX data will be compared with the results obtained with the Raman spectrometer RLS during the ExoMars2022 mission on the surface of Mars. All this taken together, it helps to better understand the origin of its moons.

Science with the miniaturized radiometer (miniRAD)

The miniaturized Radiometer (miniRAD) aims at investigating the surface temperature of Phobos by measuring the radiative flux emitted in the thermal infrared wavelength range using thermopile sensors (Kessler et al. 2005). The instrument, which will be mounted in the front compartment of the rover, has strong heritage from the Rosetta MUPUS thermal mapper (Spohn et al. 2007), the MASCOT radiometer (Grott et al. 2017), and the InSight radiometer (Spohn et al. 2018; Müller et al. 2020). The six miniRAD sensors have a field of view of 45° and will observe a spot at a distance of ∼25 to ∼150 cm in front of the rover, which will be located within the field of view of the stereo navigation cameras (navCAMs, see Sec.). In this way, geological context for the miniRAD observations will be provided along with a digital terrain model of the scene.

The surface temperatures T on Phobos are governed by the surface energy balance, which is driven by insolation S and given by

$$\sigma_B \varepsilon T^4 = (1 - A)S + \Gamma \sqrt{\frac{\pi}{P}} \left. \frac{\partial T}{\partial z'} \right|_{z'=0} \quad (1)$$

where σ_B is the Stefan-Boltzmann constant, ε is surface emissivity, A is bond albedo, P is Phobos' rotation period, and $z' = z/d$ is depth z normalized to the skin depth $d = \sqrt{kP/\rho c_p \pi}$. Here, ρ is the material's bulk density, c_p is heat capacity, and k is thermal conductivity. In Eq. 1, the thermal inertia

$$\Gamma = \sqrt{k \rho c_p} \quad (2)$$

is the material parameter governing the surface's temperature response to heating, where low values of Γ correspond to fast changes and vice versa. Therefore, given surface emissivity as well as surface temperature, the material's thermophysical parameters can be estimated (Hamm et al. 2018).

Phobos' thermal inertia was first estimated from Viking orbiter data (Lunine et al. 1982), and values between 25 and 85 J m^{-2} K^{-1} s$^{-1/2}$ were determined. Interpretation of Phobos 2 data yielded similarly low results in the 33 to 83 J m^{-2} K^{-1} s$^{-1/2}$ range (Ksanfomality et al. 1989), and estimates taking surface roughness into account derived thermal inertias between 20 and 40 J m^{-2} K^{-1} s$^{-1/2}$ using the same data set (Kuehrt and Giese 1989; Kuehrt et al. 1992). Spatially resolved thermal inertia maps were first derived from Mars Global Surveyor thermal emission spectrometer (TES) measurements (Smith et al. 2018), and a globally averaged thermal inertia of 70 J m^{-2} K^{-1} s$^{-1/2}$ was obtained. There is some evidence for regions with thermal inertias larger than 100 J m^{-2} K^{-1} s$^{-1/2}$ in the TES data (Smith et al. 2018), and some regions with anomalously high thermal inertia were also reported based on Phobos 2 data (Ksanfomality et al. 1989; Kuzmin and Zabalueva 2003), indicating at least some spatial heterogeneity with respect to surface thermophysical properties and potentially rock abundance. Furthermore, data provided by the Mars Odyssey THEMIS instrument (Bandfield et al. 2018) seems to be best compatible with a layered regolith structure, and models considering a several centimeter thick cover of fine regolith with thermal inertia of 50 J m^{-2} K^{-1} s$^{-1/2}$ above a consolidated layer with inertias of 1000 J m^{-2} K^{-1} s$^{-1/2}$ best reproduce the observations.

The above range of thermal inertias corresponds to thermal conductivities between 0.00076 and 0.023 W m^{-1} K^{-1} (Kuzmin and Zabalueva 2003), which can be compared to estimates obtained for other small bodies. Fig. 4 shows thermal conductivity as a function of temperature for Phobos as well as C-class asteroids, S-class asteroids, average near Earth asteroids, and comets. The thermal conductivity of the

lunar regolith is shown as a reference. While surface thermal conductivity on most minor bodies exceeds 0.025 W m^{-1} K^{-1}, the current best estimate for Phobos is only 0.007 W m^{-1} K^{-1} and thus similar to the lunar value of 0.003 W m^{-1} K^{-1}. This has generally been interpreted in terms of a surface cover of fine grained regolith with average particle diameters in the few millimeter range (Gundlach and Blum 2013). Furthermore, the reported low thermal conductivity indicates a low surface rock abundance in the few percent range.

The interpretation of the available thermal infrared data for Phobos is complicated by the fact that to date, all available data-sets cover only a limited range of local times. However, the influence of, e.g., surface roughness (Kuehrt et al. 1992) or layering is best studied considering the entire diurnal temperature curve. Surface roughness strongly affects thermal emission on airless bodies (Kuehrt et al. 1992; Davidsson et al. 2015), and its effect on emitted flux is shown in Fig. 5, where the ratio of the flux emitted by a rough surface to that emitted by a flat Lambertian surface is shown as a function of solar zenith angle. The employed roughness model (Giese and Kuehrt 1990; Kuehrt et al. 1992; Lagerros 1996) considers a surface covered by hemispherical craters, a crater density of 50%, a bond albedo of 0.02, an emissivity of 0.95, and a heliocentric distance of 2 AU. As is evident from the figure, roughness can dramatically change the flux received by the instrument when compared to a flat surface, and this effect is most pronounced at short wavelengths under low sun conditions. Therefore, observing temperatures for a full day-night cycle over the entire range of solar incidence angles provides data that can help to resolve some of the inherent ambiguities when interpreting received flux in terms of surface temperatures. Furthermore, measurements at different wavelengths can help to disentangle surface roughness from thermal inertia.

The sensing depth of thermal infrared observations is of the order of a few diurnal skin depths d. The latter is expected to be close to 5 mm for Phobos' regolith and of the order of a few centimeters for typical boulders. Therefore, shallow regolith layering or the presence of a thin veneer of low thermal inertia dust covering bedrock or boulders should be detectable by thermal infrared measurements. Layering has a pronounced effect on surface temperatures (Biele et al. 2019; Grott et al. 2019), and cooling rates after sunset are particularly sensitive. Therefore, data covering full diurnal temperature cycles can be used to constrain the presence or absence of layering, as has been done for a boulder on asteroid Ryugu during its visit by the JAXA Hayabusa2 spacecraft using the lander MASCOT radiometer data (Grott et al. 2019).

The miniRAD instrument onboard the MMX rover will observe the surface of Phobos in 6 distinct wavelength bands and investigate different geological units along the rover's traverse. Surface temperatures of fine grained regolith as well as boulders will be determined for full diurnal cycles, thus enabling interpretation of the data in terms of thermophysical properties, roughness, and layering. For granular material, miniRAD will determine regolith thermal conductivity, porosity, and particle size (Ogawa et al. 2019), while for boulders, thermal conductivity as well as porosity can be determined. The miniRAD data will be diagnostic for determining the potential presence of thin dust covers on boulders, and the influence of surface roughness will be quantified by observing the same target in different wavelength bands. In this way, material properties can be determined and directly compared to those of other small bodies and known meteorites (Flynn et al. 2018), shedding light on the moon's formation and evolution processes.

Science with the Navigation Cameras (NavCams)

The NavCams are a set of stereo cameras (two cameras, aligned on a bench) observing the landscape in front of the rover (Fig. 6). As their name indicates, their purpose is to allow both for the navigation of the rover and its progression, autonomously or commanded from ground, on the possibly rough terrain of Phobos and performing unprecedented science at the surface of Phobos.

The cameras are based on a microcamera cube CMV-4000 developed by CNES and 3DPLUS company. The image sensor consists of a 2048 by 2048 array (4 Mpixel), with each pixel having a 5.5μm pitch. It is based on a pinned photodiode to reach low noise and high electro-optic performances. For the NavCams, this microcamera cube is equipped with a color image sensor (Bayer filter, i.e. forming a RGGB 2x2 mosaic that repeats across the detector). The optics lead to a field-of-view of 118° in diagonal and 83° edge-to-edge, and a depth-of-field allowing to acquire images of the surface from 35 cm up to infinity. At 1 m distance the spatial resolution is about $\sim$ 1 mm per pixel.

Beyond the identification of areas of interests, the NavCam images will allow the characterization of the surface topography and morphologies at high spatial resolution as well as the determination of the spatial distribution of the blue and red materials already detected at a lower spatial resolution on Phobos (e.g., Thomas et al. 2011; Pieters et al. 2014). To fulfil these scientific objectives, we will rely on the generation of 1) geo-referenced digital terrain models (DTMs), 2) albedo maps, and 3) low resolution spectral maps. In particular, the NavCams' observations will allow progress to be made in our understanding of the origin of the blue and red materials. As of today, no simple spatial distribution nor stratigraphic relation

between these materials can be discerned (Pieters et al. 2014). There is also no apparent color-age relation for small craters: fresh (recent) craters expose either type of material at different locations (Pieters et al. 2014). Given the observed spatial relationships, it is currently difficult to formulate a single model through which the red unit is largely a depositional unit or is derived from the blue unit by some form of space weathering.

In addition, the local high resolution DTMs will be geo-referenced to the global DTM of Phobos reconstructed from the orbiter camera (TENGOO). The unprecedented resolution of the local DTMs will allow us to identify and characterize small scale topographic features such as grains, boulders and cracks. These DTMs will allow the size distribution of the grains to be constrained down to 1 mm and tentatively allow monitoring any regolith movement and albedo variation on short timescales. They will be a key complement to the geomorphologic analyses performed with the orbiter camera observations for the whole surface and will allow us to refine our understanding of the overall geological history of Phobos.

Science with the Wheel Cameras (WheelCams)

The WheelCams are a set of two cameras placed on the underside of the rover and each aimed at a different wheel (Fig. 7). Their primary purpose is to observe the wheels and the behavior of the regolith around the wheels as the rover is advancing on Phobos, providing unique information on the dynamics of the regolith in the low-gravity environment of Phobos. Their secondary purpose is to provide colour images at very high resolution of the Phobos soil.

The cameras are based on the same microcamera cube as the NavCams (see previous section). However, the detector is panchromatic (no colour filter). The optics provide a field of view of 32.5°, a best focus distance of 35 cm and a field depth of 10 cm. This gives a pixel resolution of approximately 70 μm at the center of the image.

In order to illuminate the scene, which is almost always in the shadow of the rover body and solar panels, they are equipped with LEDs. Some are "high power" (0.5 W) white LEDs to be used while driving, while others are colour LEDs of specific bandwidths to allow for multispectral imaging. These colour LEDs are from the Euclid mission (ESA): the L-590, the L-720 and the EOLD-880 at respectively 590 nm, 720 nm and 880 nm (Boutillier et al. 2014).

The cameras can be used with the white LED while the rover is driving (typical image frequency will be about one picture every second for a motion of about 1 mm/s), or at night with the color LEDs and with

longer exposure times. Because of the huge data volumes produced by the image sequences, they are binned down to 1024 by 1024 images and cropped to retain only the most important part of the picture. Temporal compression if the image sequences is also considered, but not confirmed at this stage. On the other hand, the detailed night images with the color LEDs are transmitted with lossless compression (no binning or cropping).

The physical properties of Phobos' surface are closely linked to the history and origin of the body. Such information also has important implications for spacecraft - surface interactions such as the landing of the main MMX spacecraft and the surface sampling. Given that remote observations can often lead to very different interpretations on surface and internal properties, the only way to truly probe the mechanical and physical properties is to directly interact with the surface material. By observing the surface and the interactions between the rover wheels and the regolith, the WheelCams will study the mechanical and dynamical properties of Phobos' regolith.

The WheelCams will be used to characterise the general grain properties of Phobos' regolith. Specifically, the high resolution WheelCam images will allow the regolith particles to be identified down to particle sizes of approximately 200 μm. Combining this information with local high resolution DTMs from the NavCams, and images and global DTMs from the main MMX spacecraft will provide the particle size distribution, spanning many more orders of magnitude than previous studies of Phobos (Thomas et al. 2000). The slope of the particle size distribution can indicate how much processing (impacting, breaking, size sorting, transporting) Phobos' regolith has experienced. The grain morphologies (sphericity and angularity) will also be investigated (for grains $>$ 1 mm) using the WheelCam images.

The rover wheel – regolith interactions will also be investigated in detail; the WheelCams will determine the depth of the wheel sinkage, which is closely linked to the load bearing strength and friction angle of the regolith (Sullivan et al. 2006). Observations of talus in the rover tracks (Sullivan et al. 2006) and tailings behind the wheels provide measurements of the angle of repose, and undisturbed trench walls provide a lower limit to the regolith cohesion (Sullivan et al. 2011). In addition, measurement of traction and slippage (e.g. Maimone et al. 2007; Reina et al. 2006) will provide shearing characteristics of the regolith. These numerous observations will be compiled in order to characterise the bulk properties of the regolith, and to improve our understanding of granular flow on Phobos and in reduced-gravity environments in general, with profound implications on Phobos' surface history.

Numerical modeling for supporting rover dynamics and interpreting regolith properties

The instruments onboard the MMX rover will provide substantial information on the small scale topographic features and grain properties of Phobos' surface. The dynamical behaviours of regolith materials both in quasi-static and flow regimes will be intensively characterised by the WheelCams. However, as the first rover rolling in a milli-gravity environment, the established knowledge about rover dynamics and regolith compliance from the Moon and Mars exploration and Earth laboratory experiments would not be applicable to interpret this information. Recent small body missions (i.e., Hayabusa2 and OSIRIS-REx) have showed that the responses of these airless, low-gravity small-body surfaces to robotic maneuvers are significantly different from those observed in an Earth-gravity environment (Arakawa et al. 2020; Bierhaus et al. 2020).

As an effective test bed for various physical properties and dynamical processes, numerical modeling is crucial to the design of the locomotion system and potentially other platform systems. Simulations are also required to help with the processing of the WheelCam images and determine the mechanical properties of the regolith. The calibrated material model and parameters can be further used to simulate the geophysical evolution of Phobos over its lifetime. Combined with the regolith mineralogical composition and thermal properties measured by the RAX and miniRad instruments,respectively, numerical modeling will help to constrain the origin and evolution of Phobos.

To fulfill the above science objectives, at least two complementary numerical approaches, with discrete and continuum treatments respectively, will be used to study the rover and regolith dynamics.

Soft-sphere Discrete Element Method (SSDEM)

The soft-sphere discrete element method (SSDEM) is a highly accurate but costly option for studying rover interactions with granular surfaces. In this method, the overall behavior of the system is determined by calculating the contact forces acting on each grain in a regolith bed and then advancing the system accordingly. Contacts are evaluated at small time intervals, where the size of the time-step is dependent on the properties of the grains. In general, stiffer surface materials will result in smaller time-steps and longer processing times. A key benefit of SSDEM is that this method effectively captures the influence of gravity and cohesion on granular flows without relying on empirical or semi-empirical relationships. SSDEM has proven to be an effective tool for advancing research related to the formation and evolution of small bodies (Sanchez and Scheeres 2014; Zhang and Lin 2020; Michel et al. 2020). This method has also been used to assess the performance of planetary rovers, though most commonly for the gravity

environments found on the moon and Mars (Nakashima et al. 2007; Johnson et al. 2015). Currently, DLR is using DEM combined with machine learning to assist with the design and optimization of the MMX rover wheel for Phobos-like surface conditions (Buchele and Lichtenheldt 2020).

A significant challenge associated with DEM is selecting the appropriate simulation parameters when the material properties of the surface are largely unknown. For the rover studies, simulations can be conducted for the entire range of soil cases presented in the previous section presenting the soil and grain mechanical environment. Then, the results can be used to create a map between observable outcomes like trench shape, wheel sinkage, and wheel slip, and important material properties like those discussed in the section presenting the science of the Wheelcams, such as cohesion and internal friction.

Fig. 8 provides an example of a typical simulation with a simplified rover wheel and a bed of large, spherical particles. In addition to wheel sinkage, the grain-scale resolution of DEM allows us to observe the shear-band created by the granular flow under the wheel.

Continuum method

A continuum description of dense granular materials can be used as a fast and coarse approach to model the rheology of granular beds. In this type of description, local particle velocities are averaged, resulting in a continuous velocity field (Da Cruz et al. 2005). Additionally, forces between particles are averaged up to viscous stress and pressure fields, similar to the Navier-Stokes equation for viscous fluids.

A first version of a continuous model for dense granular flows was proposed by Jop et al. (2006), based on the expression of an apparent (in the macroscopic sense) friction coefficient μ. This model makes it possible to reproduce the viscoplastic effects and the dependence on normal stresses observed experimentally and numerically using discrete numerical simulations (Da Cruz et al. 2005), such as the existence of a flow threshold, the dependence of μ on speed, pressure, size and density of grains. In this model, the apparent friction is an increasing function of a single parameter I, called an inertial number, defined by $I = \dot{\gamma}d/(P/\rho)^{0.5}$, where $\dot{\gamma}$, d, P and ρ are, respectively, the second invariant of the strain rate tensor, the mean particle diameter, the confining (macroscopic) pressure and the grain density. This parameter measures the relative contribution of the inertial (or kinetic) pressure to the confining (static) pressure.

This so-called $\mu(I)$ model has been successfully applied to predict rheometric shear flows, stationary one- and two-dimensionnal free surface flows (GDR MiDi group 2004) as well as three-dimensional transient free surface flows (Valette et al. 2019), using numerical simulations.

Recent extensions of the $\mu(I)$ model, such as the one proposed by Vo et al. (2020), make it possible to take into account in the same formalism both cohesive and viscous effects. In this continuous model again, the number of parameters is restricted, and will allow us to quickly explore several conditions for rover interactions with the granular bed. Subsequent inverse mapping of continuum to SSDEM models parameters can then accelerate the fine processing of WheelCam images using SSDEM.

Conclusions and Outlook

The MMX mission will provide the first detailed information on Phobos, and the first sample of a martian moon for analysis in laboratories on Earth. The rover that the spacecraft will deploy on Phobos' surface will obtain the first in-situ information on the compositional and physical properties of the surface of this moon as well as on the dynamics of regolith in the corresponding gravitational environment. Direct measurements of the surface response to an external action, such as the rolling of rover's wheels, are of unique value both for science and technical purposes. Comparison between microscale properties measured by the rover and macroscale ones measured by the instruments onboard the spacecraft, as well as the sample analyses will be of high value and will allow the maximum science return of the mission to be achieved.

After finishing Phase B in 2020 the rover will go through a full qualification program. The flight model will be delivered to Japan in 2023, to be integrated to the main MMX spacecraft where a combined testing program is foreseen. The MMX mission is planned to be launched in 2024. After arrival at Phobos, remote investigations will start, which will include landing- and sampling site selections. The rover will then be delivered to the surface of Phobos in 2026 or early 2027 and is planned to operate on Phobos for at least 100 days. Telemetry and Commands will be relayed via the mother spacecraft. There are dedicated Rover Operations centers at DLR in Cologne/Germany and at CNES in Toulouse/France. MMX will leave Mars orbit in 2028 and return to Earth in August 2029 (Kawakatsu et al. 2019) with Phobos samples.

Availability of data and materials

Not applicable.

Competing interests

Not applicable

Funding

This work benefits from funding by CNES and DLR. CS acknowledges PhD thesis funding from ISAE-SUPAERO and CNES. Y.Z. acknowledges funding from the Université Côte d'Azur "Individual grants for young researchers" program of IDEX JEDI.

Authors' contributions

The authors wish it to be known that, in their opinion, the first two authors (PM and SU) should be regarded as joint First Authors.

Acknowledgments

The rover on the MMX mission of JAXA is a CNES-DLR cooperation. The authors would like to thank the whole MMX team at JAXA/ISAS for the unique opportunity to participate to this exciting mission.

References

Arakawa M, Saiki T, Wada K, Ogawa K, Kadono T, Shirai K, et al. (2020) An artificial impact on the asteroid (162173) Ryugu formed a crater in the gravity-dominated regime. Science 368: 67–71

Bandfield JL and 9 colleagues (2018) Mars Odyssey THEMIS Observations of Phobos: New Spectral and Thermophysical Measurements. Paper presented at the 49th Lunar and Planetary Science Conference 2018, (LPI Contrib. No. 2083)

Biele J and 8 colleagues (2019) Effects of dust layers on thermal emission from airless bodies. Progress in Earth and Planetary Science 6: 48. doi:10.1186/s40645-019-0291-0

Bierhaus EB, Songer JT, Clark BC, Dubisher RD, Deden SL, Payne KS, et al. (2020) Bennu regolith mobilized by TAGSAM: Expectations for the OSIRIS-REx sample collection event and application to understanding naturally ejected particles. Icarus 355: 114–142

Boutillier M, Gilard O, Quadri G, Lhuillier S, How LS, Hernandez S (2014) Commercial Light Emitting Diodes Sensitivity to Protons Radiations. Paper presented in 2014 IEEE Radiation Effects Data

Workshop (REDW)

Buchele F, Lichtenheldt R (2020) Multi-parameter rover wheel and grouser optimization for deployment in Phobos' milli-g environment. In: iSAIRAS 2020: International Symposium on Artificial Intelligence, Robotics and Automation in Space. iSAIRAS 2020, 19–23.10.2020, virtual online

Cho Y, Rull F, Böttger U and the RAX Team (2020) In-situ science on Phobos with the Raman spectrometer RAX onboard the MMX rover. This issue

Da Cruz F, Emam S, Prochnow M, Roux JN, Chevoir F (2005) Rheophysics of dense granular materials: Discrete simulation of plane shear flows. Physical Review E 72: 021309

Davidsson BJR, Gutiérrez PJ, Rickman H (2009) Physical properties of morphological units on Comet 9P/Tempel 1 derived from near-IR Deep Impact spectra. Icarus 201: 1, 335-357. doi:10.1016/j.icarus.2008.12.039

Davidsson BJR, Rickman H, Bandfield JL, Groussin O, Gutiérrez PJ, Wilska M, Capria MT, Emery JP, Helbert J, Jorda L, Maturilli A, Mueller TG (2015) Interpretation of thermal emission. I. The effect of roughness for spatially resolved atmosphereless bodies. Icarus 252: 1-21. doi:10.1016/j.icarus.2014.12.029

Delbo' M, dell'Oro A, Harris AW, Mottola S, Mueller M (2007) Thermal inertia of near-Earth asteroids and implications for the magnitude of the Yarkovsky effect. Icarus 190: 236-249. doi:10.1016/j.icarus.2007.03.00

Dellagiustina DN and 58 colleagues (2019) Properties of rubble-pile asteroid (101955) Bennu from OSIRIS-REx imaging and thermal analysis. Nature Astronomy 3: 341-351. doi:10.1038/s41550-019-0731-1

Emery JP. and 8 colleagues (2014) Thermal infrared observations and thermophysical characterization of OSIRIS-REx target asteroid (101955) Bennu. Icarus 234: 17-35. doi:10.1016/j.icarus.2014.02.005

Flynn GJ, Consolmagno GJ, Brown P, Macke RJ (2018) Physical properties of the stone meteorites: Implications for the properties of their parent bodies. Chemie der Erde Geochemistry 78: 269-298. doi:10.1016/j.chemer.2017.04.002

Fujiwara A and 21 colleagues (2006) The Rubble-Pile Asteroid Itokawa as Observed by Hayabusa. Science 312: 1330-1334. doi:10.1126/science.1125841

GDR MiDi group (2004) On dense granular flows. European Physical Journal E 14: 341–365

Giese B, Kuehrt E (1990) Theoretical interpretation of infrared measurements at Deimos in the

framework of crater radiation. Icarus 88: 372-379. doi:10.1016/0019-1035(90)90088-Q

Giuranna M and 6 colleagues (2011) Compositional interpretation of PFS/MEx and TES/MGS thermal infrared spectra of Phobos. Planetary and Space Science 59: 1308-1325. doi:10.1016/j.pss.2011.01.019

Grott M and 7 colleagues (2017) The MASCOT Radiometer MARA for the Hayabusa 2 Mission. Space Science Reviews 208: 413-431. doi:10.1007/s11214-016-0272-1

Grott M and 36 colleagues (2019) Low thermal conductivity boulder with high porosity identified on C-type asteroid (162173) Ryugu. Nature Astronomy 3: 971-976. doi:10.1038/s41550-019-0832-x

Groussin O and 15 colleagues (2013) The temperature, thermal inertia, roughness and color of the nuclei of Comets 103P/Hartley 2 and 9P/Tempel 1. Icarus 222: 580-594. doi:10.1016/j.icarus.2012.10.003

Gundlach B, Blum J (2013) A new method to determine the grain size of planetary regolith. Icarus 223: 479-492. doi:10.1016/j.icarus.2012.11.039

Hamm M, Pelivan I, Grott M, de Wiljes J (2020) Thermophysical modelling and parameter estimation of small Solar system bodies via data assimilation. Monthly Notices of the Royal Astronomical Society 496: 2776-2785. doi:10.1093/mnras/staa1755

Hamm M, Grott M, Kuehrt E, Pelivan I, Knollenberg J (2018) A method to derive surface thermophysical properties of asteroid (162173) Ryugu (1999JU3) from in-situ surface brightness temperature measurements. Planetary and Space Science 159: 1-10. doi:10.1016/j.pss.2018.03.017

Harris AW, Davies JK (1999) Physical Characteristics of Near-Earth Asteroids from Thermal Infrared Spectrophotometry. Icarus 142: 464-475. doi:10.1006/icar.1999.6248

Hayne PO and 10 colleagues (2017) Global Regolith Thermophysical Properties of the Moon From the Diviner Lunar Radiometer Experiment. Journal of Geophysical Research (Planets) 122: 2371-2400. doi:10.1002/2017JE005387

Johnson JB, Kulchitsky AV, Duvoy P, Iagnemma K, Senatore C, Arvidson RE, Moore J (2015) Discrete element method simulations of Mars Exploration Rover wheel performance. Journal of Terramechanics 62: 31–40

Jop P, Forterre Y, Pouliquen O (2006) A constitutive law for dense granular flows. Nature 441: 727–730

Kawakatsu Y, Kuramoto K, Ogawa N, Ikeda H, Ono G, et al. (2019) Mission Definition of Martian Moon Exploration (MMX), 70th International Astronautical Congress, IAC-19-A3.4.B7

Kessler E, *Proc. of Sensor 2005 12th International Conference*, Vol. I, Nürnberg, 73-78 (2005)

Ksanfomality LV and 9 colleagues (1989) Spatial variations in thermal and albedo properties of the

surface of Phobos. Nature 341: 588-591. doi:10.1038/341588a0

Ksanfomality LV and 15 colleagues (1991) Phobos: Spectrophotometry between 0.3 and 0.6 μm and IR-radiometry. Planetary and Space Science 39: 311-326. doi:10.1016/0032-0633(91)90152-Z

Kuehrt E, Giese B (1989) A thermal model of the Martian satellites. Icarus 81: 102-112. doi:10.1016/0019-1035(89)90128-0

Kuehrt E, Giese B, Keller HU, Ksanfomality LV (1992) Interpretation of the KRFM-infrared measurements of Phobos. Icarus 96: 213-218. doi:10.1016/0019-1035(92)90075-I

Kuramoto K, Kawakatsu Y, Fujimoto M and MMX study team, Martian Moon Exploration (MMX) (2017) Conceptual Study Results, Lunar and Planetary Science Conference XLVIII, Abstr. 2086

Kuzmin RO, Zabalueva EV (2003) The Temperature Regime of the Surface Layer of the Phobos Regolith in the Region of the Potential Phobos-Grunt Space Station Landing Site. Solar System Research 37: 480-488. doi:10.1023/B:SOLS.0000007946.02888.bd

Lagerros JSV (1996) Thermal physics of asteroids. I. Effects of shape, heat conduction and beaming. Astronomy and Astrophysics 310: 1011-1020

Lebofsky LA, Rieke GH (1979) Thermal properties of 433 Eros. Icarus 40: 297-308. doi:10.1016/0019-1035(79)90074-5

Lichtenheldt R, Barthelmes S, Buse F, Hellerer M (2016) Wheel-Ground Modeling in Planetary Exploration: From Unified Simulation Frameworks Towards Heterogeneous, Multi-tier Wheel Ground Contact Simulation. In: Font-Llagunes J. (eds) Multibody Dynamics. Computational Methods in Applied Sciences, vol 42. Springer, Cham

Lorenz RD (2020) How far is far enough? Requirements derivation for planetary mobility systems. Adv. Space Res. 65: 1383-1401

Lunine JI, Neugebauer G, Jakosky BM (1982). Infrared observations of Phobos and Deimos from Viking. Journal of Geophysical Research 87: 10297-10305. doi:10.1029/JB087iB12p10297

Maimone M, Cheng Y, Matthies L (2007) Two years of Visual Odometry on the Mars Exploration Rovers. J. Field Robotics 24: 169-186. doi:10.1002/rob.20184

Michel P, Ballouz RL, Barnouin OS, Jutzi M, Walsh KJ, May BH, Manzoni C, Richardson DC, Schwartz SR, Sugita S, et al. (2020) Collisional formation of top-shaped asteroids and implications for the origins of Ryugu and Bennu. Nature Communications, 11: 1–11. doi:10.1038/s41467-020-16433-z

Müller TG and 29 colleagues (2017) Hayabusa-2 mission target asteroid 162173 Ryugu (1999 JU_3):

Searching for the object's spin-axis orientation. Astronomy and Astrophysics 599: A103. doi:10.1051/0004-6361/201629134

Mueller NT and 8 colleagues (2020) Calibration of the HP^3 Radiometer on InSight. Earth and Space Science 7(5): e01086. doi:10.1029/2020EA001086

Nakashima H, Fujii H, Oida A, Momozu M, Kawase Y, Kanamori H, Aoki S, Yokoyama T (2007) Parametric analysis of lugged wheel performance for a lunar microrover by means of DEM. Journal of Terramechanics 44: 153–162

Ogawa K, Hamm M, Grott M, Sakatani N, Knollenberg J, Biele J (2019) Possibility of estimating particle size and porosity on Ryugu through MARA temperature measurements. Icarus 333: 318-322. doi:10.1016/j.icarus.2019.06.014

Okada T. and 78 colleagues (2020) Highly porous nature of a primitive asteroid revealed by thermal imaging. Nature 579: 518–522. doi:10.1038/s41586-020-2102-6

Pieters CM, Murchie S, Thomas N, Britt D (2014) Composition of Surface Materials on the Moons of Mars. Planetary and Space Science 102: 144-151. doi:10.1016/j.pss.2014.02.008

Ramsley KR, Head JW (2013) Mars impact ejecta in the regolith of Phobos: Bulk concentration and distribution. Planetary and Space Science 87: 115-129. doi:10.1016/j.pss.2012.10.007

Reina G, Ojeda L, Milella A, Borenstein J (2006) Wheel slippage and sinkage detection for planetary rovers. IEEE/ASME Transactions on Mechatronics 11: 185-195. doi: 10.1109/TMECH.2006.871095

Rozitis B and 14 colleagues (2019) Thermal Inertia Maps of (101955) Bennu from OSIRIS-REx Infrared Observations. EPSC-DPS Joint Meeting 2019

Sánchez P, Scheeres DJ (2014) The strength of regolith and rubble pile asteroids. Meteoritics & Planetary Science 49: 788–811

Smith NM, Edwards CS, Mommert M, Trilling DE, Glotch TD (2018) Mapping the Thermal Inertia of Phobos Using MGS-TES Observations and Thermophysical Modeling. Lunar and Planetary Science Conference

Spohn T, Seiferlin K, Hagermann A, Knollenberg J, Ball AJ, Banaszkiewicz M, Benkhoff J, Gadomski S, Gregorczyk W, Grygorczuk J, Hlond M, Kargl G, Kuehrt E, Kömle N, Krasowski J, Marczewski W, Zarnecki JC (2007) Mupus - A Thermal and Mechanical Properties Probe for the Rosetta Lander Philae. Space Science Review 128: 339-362. doi:10.1007/s11214-006-9081-2

Spohn T, Knollenberg J, Ball AJ, Banaszkiewicz M, Benkhoff J, Grott M, Grygorczuk J, Hüttig C,

Hagermann A, Kargl G, Kaufmann E, Kömle N, Kuehrt E, Kossacki KJ, Marczewski W, Pelivan I, Schrödter R, Seiferlin K (2015) Thermal and mechanical properties of the near-surface layers of comet 67P/Churyumov-Gerasimenko. Science 349: 6247. doi:10.1126/science.aab0464

Spohn T and 22 colleagues (2018) The Heat Flow and Physical Properties Package (HP^3) for the InSight Mission. Space Science Reviews 214: P24D-01

Sullivan R, Anderson R, Biesiadecki J, Bond T, Stewart H (2011) Cohesions, friction angles, and other physical properties of Martian regolith from Mars Exploration Rover wheel trenches and wheel scuffs. J. Geophys. Res. 116: E02006. doi:10.1029/2010JE003625

Sullivan R, Anderson R, Biesiadecki J, Bond T, Stewart H (2011), Cohesions, friction angles, and other physical properties of Martian regolith from Mars Exploration Rover wheel trenches and wheel scuffs. J. Geophys. Res, 116: E02006. doi:10.1029/2010JE003625

Sunday C, Murdoch N, Tardivel S, Schwartz SR, Michel P (2020) Validating N-body code CHRONO for granular DEM simulations in reduced-gravity environments. Monthly Notices of the Royal Astronomical Society 498: 1062–1079

Thomas PC, Veverka J, Sullivan R, et al. (2000) Phobos: Regolith and ejecta blocks investigated with Mars Orbiter Camera images. Journal of Geophysical Research 105: 15091–15106

Thomas N, Stelter R, Ivanov A, Bridges NT, Herkenhoff KE, McEwen AS (2011) Spectral heterogeneity on Phobos and Deimos: HiRISE observations and comparisons to Mars Pathfinder results. Planetary and Space Science 59: 1281-1292. doi:10.1016/j.pss.2010.04.018

Ulamec S, Michel P and 54 colleagues (2019), A Rover for the MMX Mission to Phobos, 70th International Astronautical Congress

Valette R, Riber S, Sardo L, Castellani R, Costes F, Vriend N, Hachem E (2019) Sensitivity to the rheology and geometry of granular collapses by using the μ(I) rheology. Computers & Fluids 191: 104260

Vo TT, Nezamabadi S, Mutabaruka P, Delenne JY, Radjai F (2020) Additive rheology of complex granular flows. Nature Communications 11: 1476

Zhang Y, Lin DNC (2020) Tidal fragmentation as the origin of 1I/2017 U1 (‘Oumuamua). Nature Astronomy 4: 852-–860

Figure 1. Left: Rover in fully deployed configurations with positions of MiniRad, rear WheelCam and NavCam stereo bench; right: internal compartment (Service Module – SEM) with position if instruments and On Board Computer (OBC). Courtesy from CNES.

Figure 2. MMX rover with deployed wheels and solar panels in the on-surface configuration. Field of Views of miniRAD and Wheelcams are indicated in yellow and red, respectively. Courtesy from CNES.

Figure 3. CAD model of RAX (Raman spectrometer for MMX).

Figure 4. Thermal conductivity as a function of temperature as derived for different small bodies. Data for C-class asteroids Bennu (Emery et al. 2014; Dellagiustina et al. 2019; Rozitis et al. 2019) and Ryugu (Müller et al. 2017; Hamm et al. 2020), for average near Earth asteroids (Delbo' et al. 2007), for comets 9P/Tempel 1 (Groussin et al. 2013; Davidsson et al. 2009), 103P/Hartley (Groussin et al. 2013), and 67P/Churyumov-Gerasimenko (Spohn et al. 2015), for S-class asteroids Itokawa (Fujiwara et al. 2006) and Eros (Lebofsky and Rieke 1979; Harris and Davies 1999) are shown together with the current best estimate for Phobos (Kuzmin and Zabalueva 2003). For comparison, the thermal conductivity of the lunar regolith (Hayne et al. 2017) is also given.

Figure 5. The ratio of flux emitted by a rough surface to that emitted by a flat Lambertian surface as a function of solar zenith angle at three different wavelengths. Results are shown for an equatorial location and a south facing instrument, which observes the surface under an emission angle of 45°.

Figure 6. The navigation cameras. Left: CAD view; right: schematic view.

Figure 7. The wheel cameras in their pre-phase A design. Left: CAD view; right: schematic view.

Figure 8. Example SSDEM simulation of a simplified MMX rover wheel traversing a bed of 180,000 cohesionless spherical grains. The wheel is 214 mm in diameter and the grains are 6 ± 0.5 mm in diameter. The simulation was conducted under Earth-gravity using Chrono (Sunday et al. 2020). The grains are colored by velocity magnitude.

Figure 1a

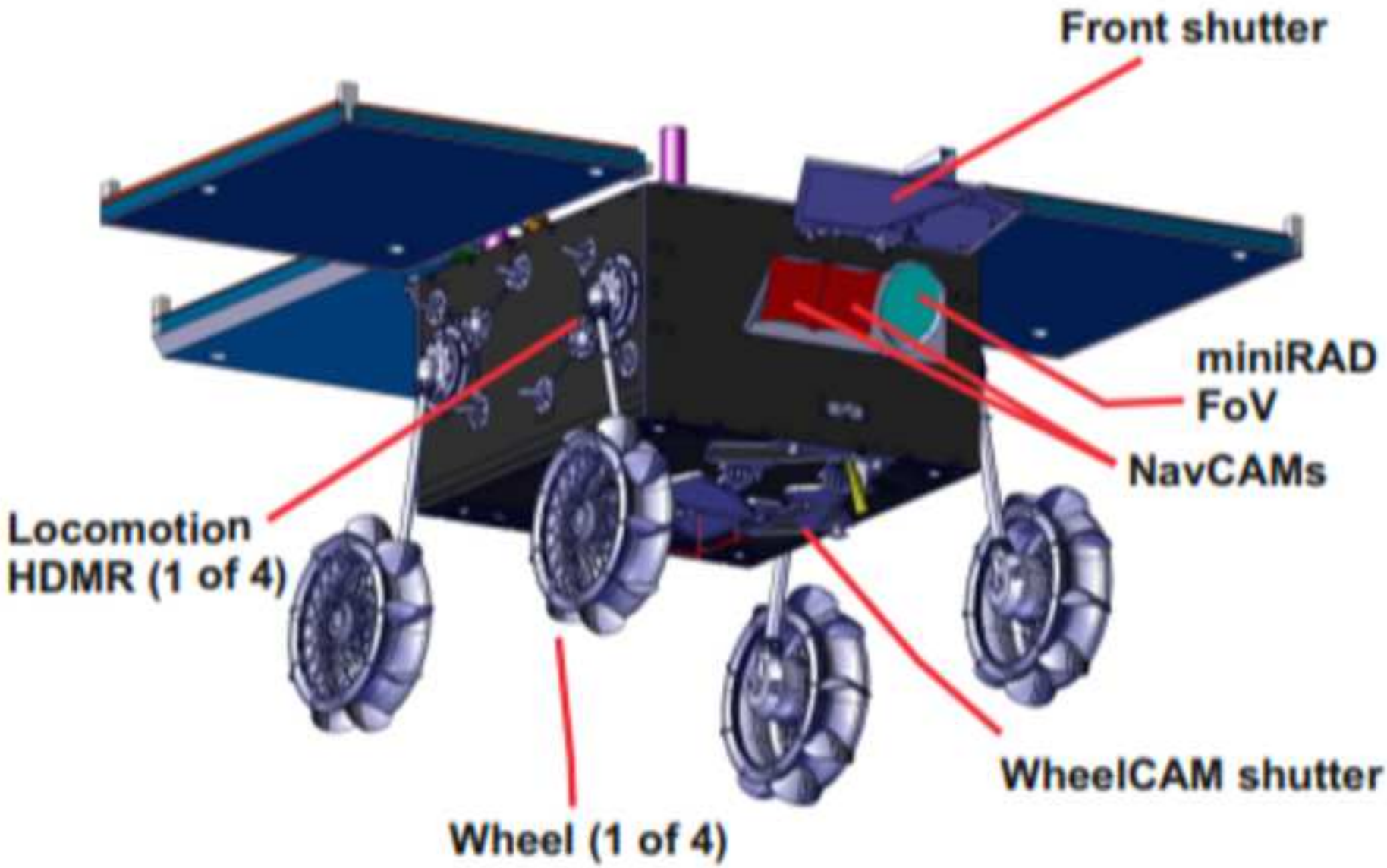
Front shutter
miniRAD
FoV
NavCAMs
Locomotion
HDMR (1 of 4)
WheelCAM shutter
Wheel (1 of 4)

Figure 1b

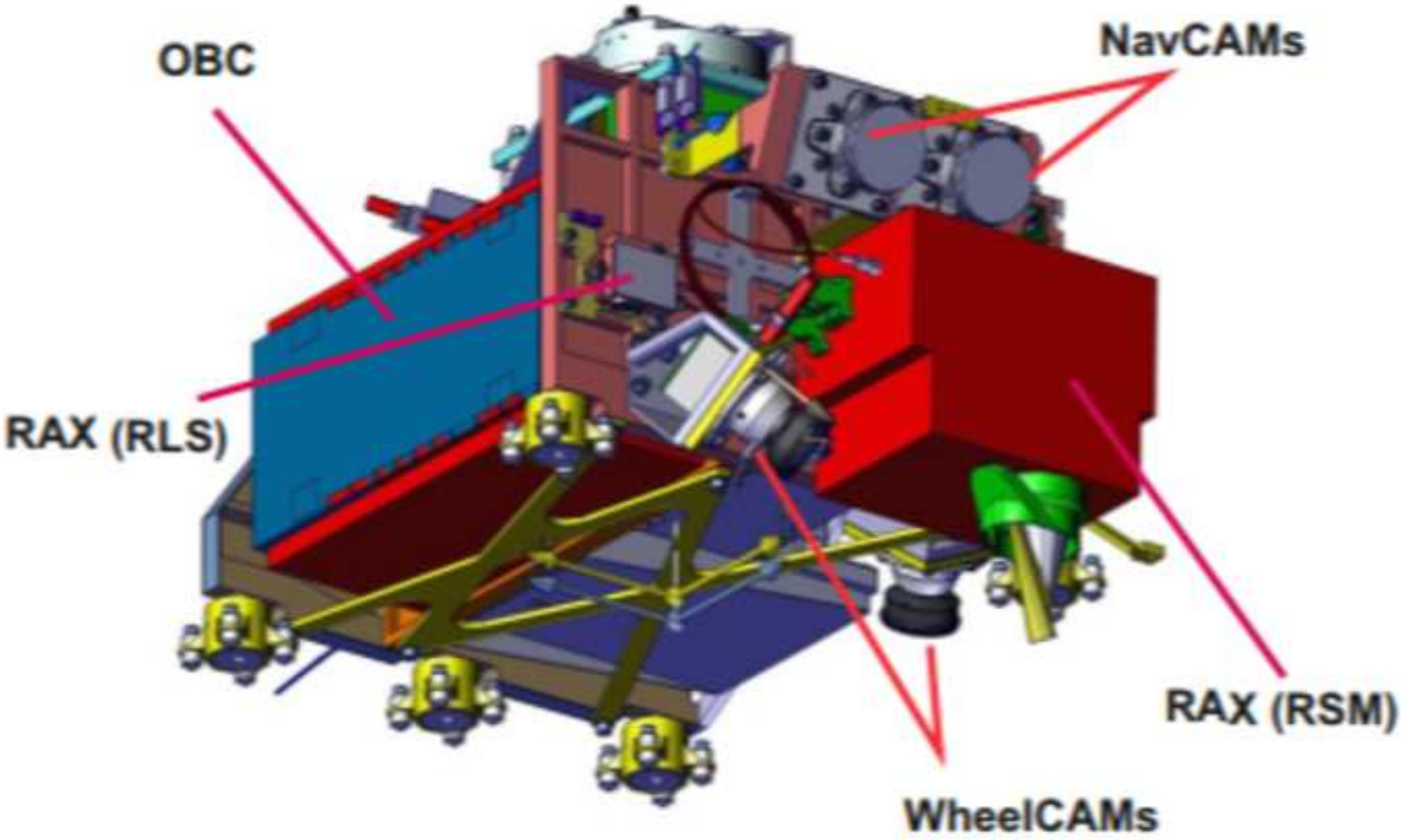

Figure 2

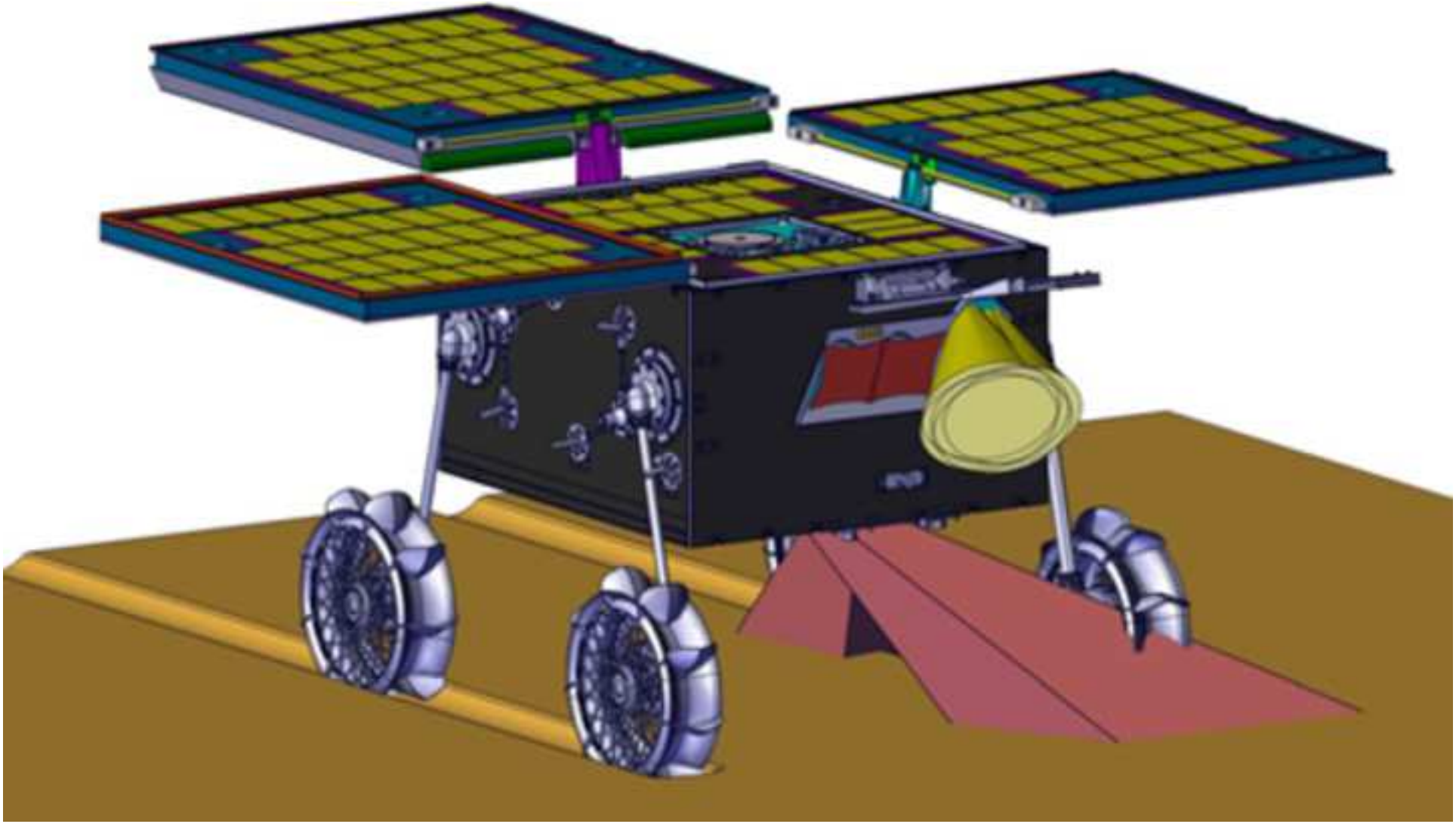

Figure 3

Figure 4

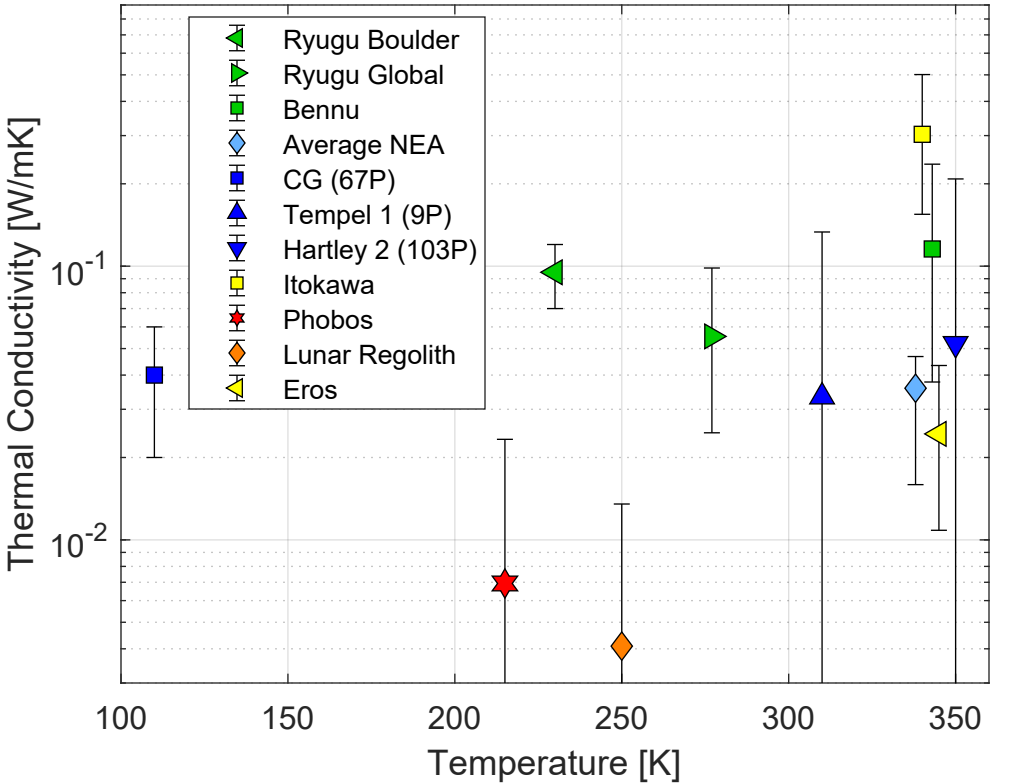
Ryugu Boulder
Ryugu Global
Bennu
Average NEA
CG (67P)
Tempel 1 (9P)
Hartley 2 (103P)
Itokawa
Phobos
Lunar Regolith
Eros
Thermal Conductivity [W/mK]
10^{-1}
10^{-2}
100
150
200
250
300
350
Temperature [K]

Figure 5

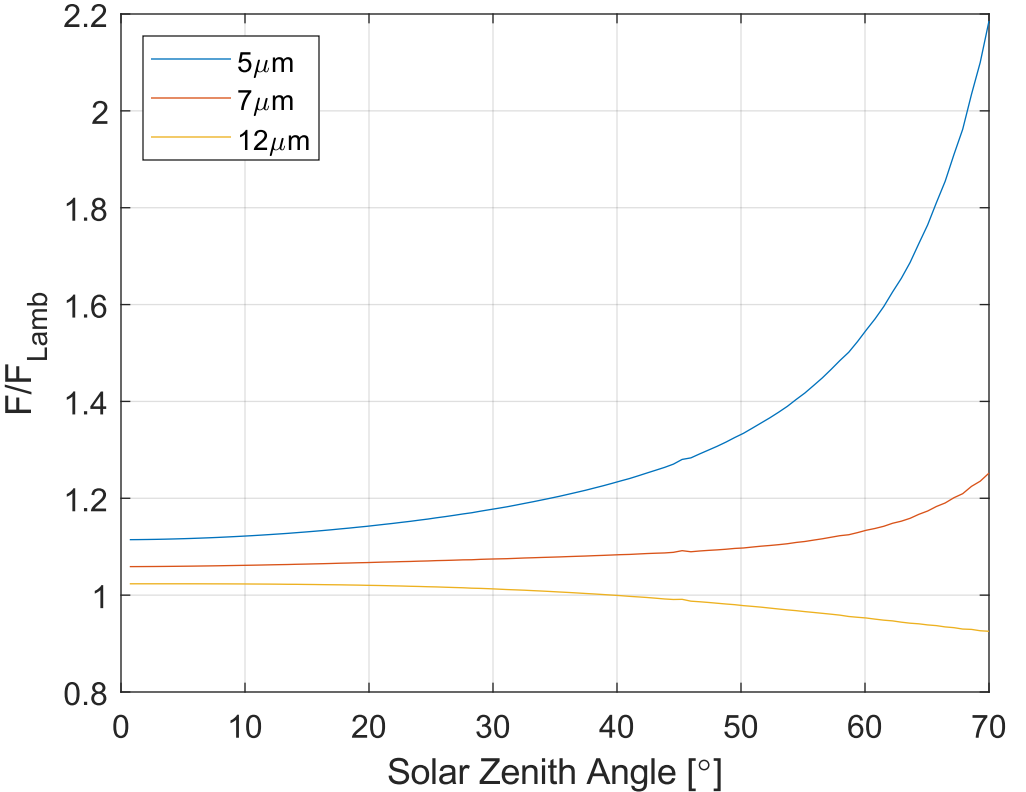
5μm
7μm
12μm
F/F_Lamb
2.2
2
1.8
1.6
1.4
1.2
1
0.8
0
10
20
30
40
50
60
70
Solar Zenith Angle [°]

Figure 6

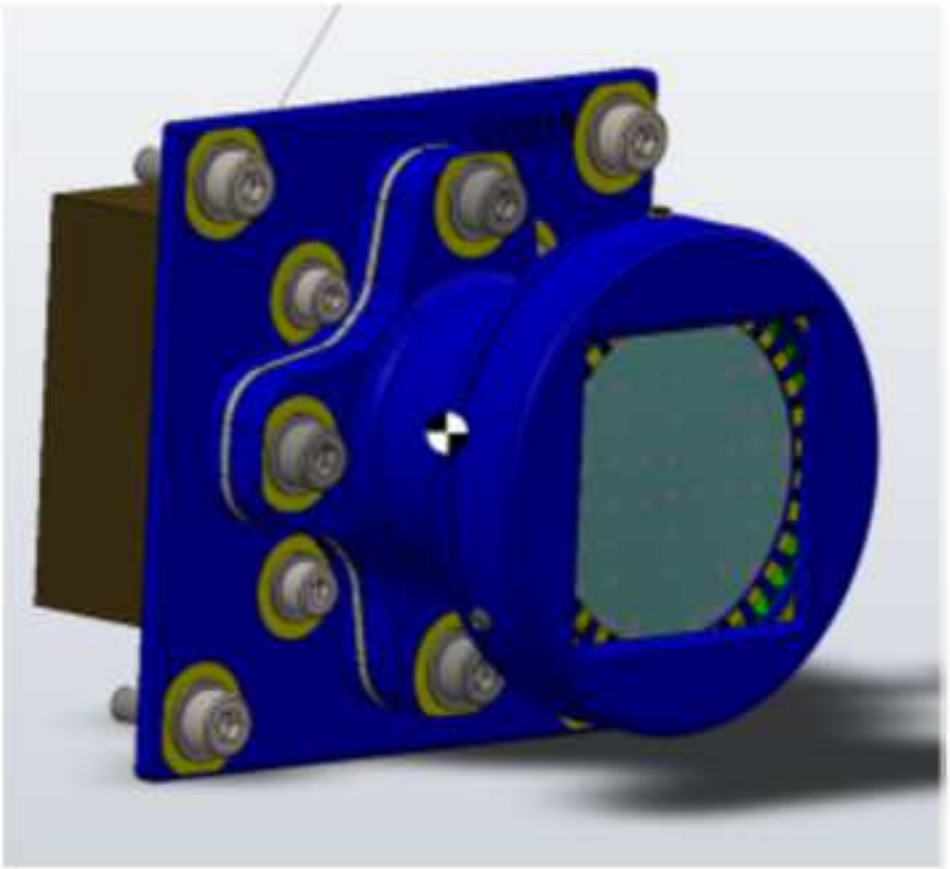

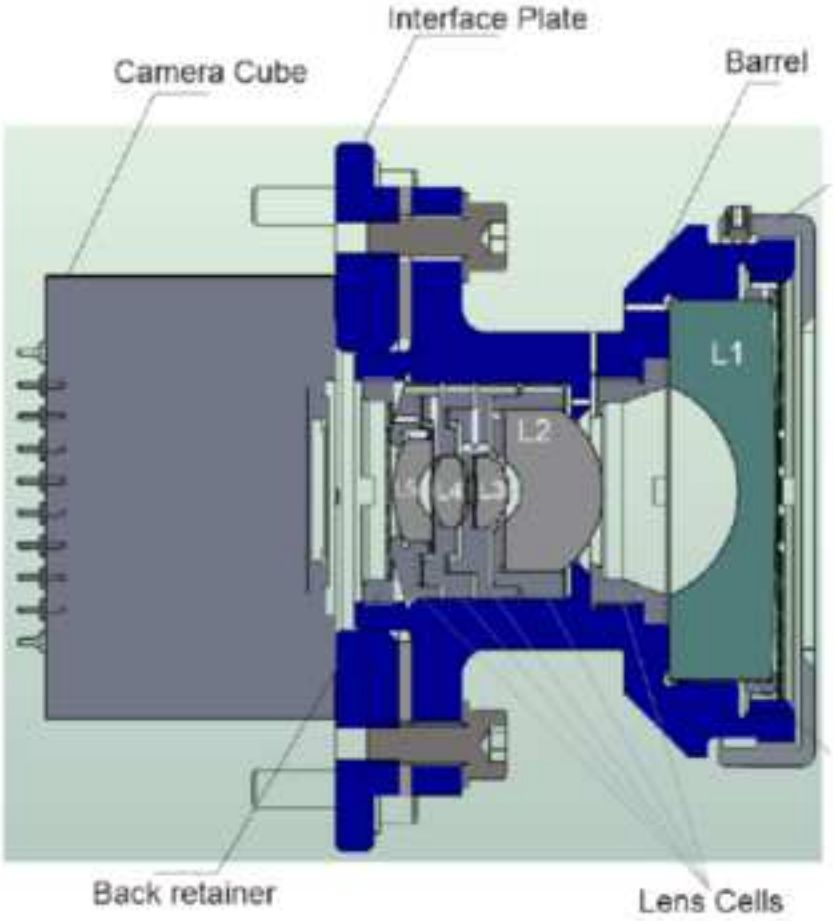
Interface Plate
Camera Cube
Barrel
L1
L2
Back retainer
Lens Cells

Figure 7

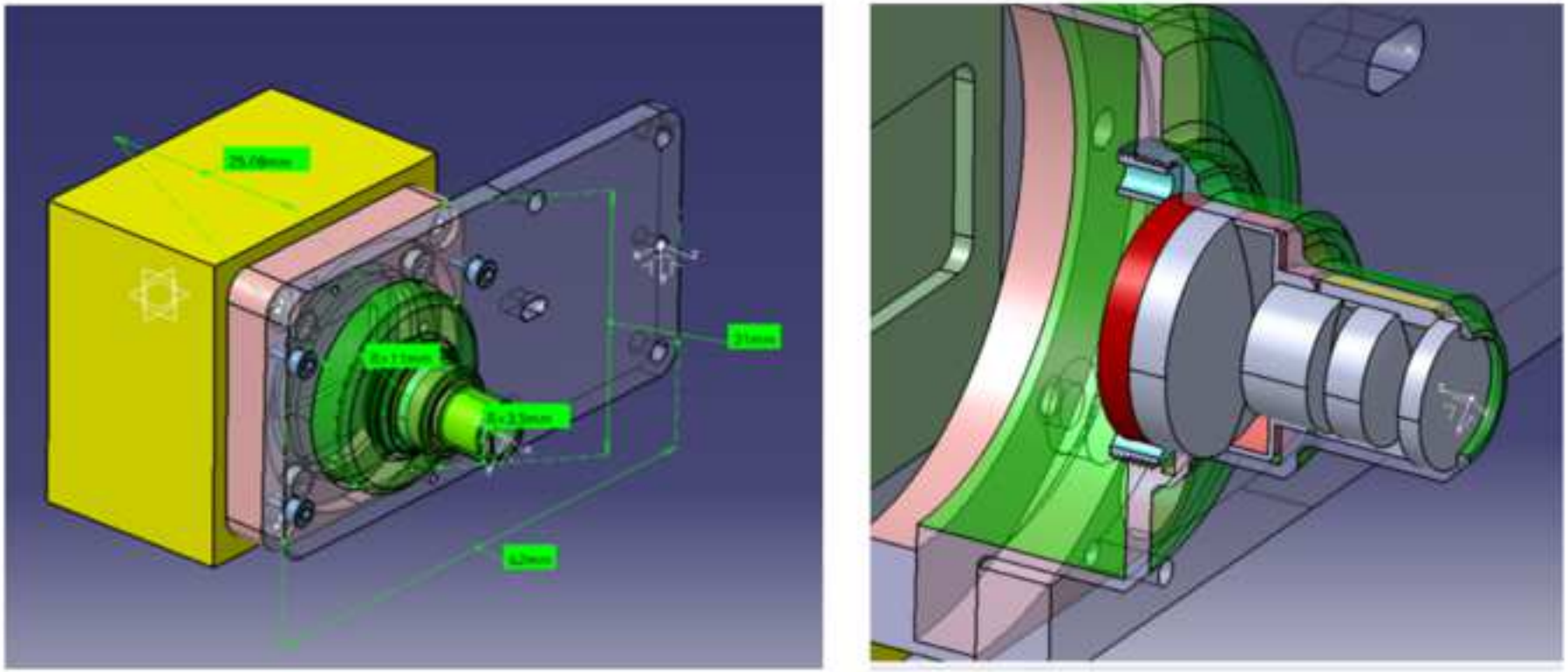

Figure 8

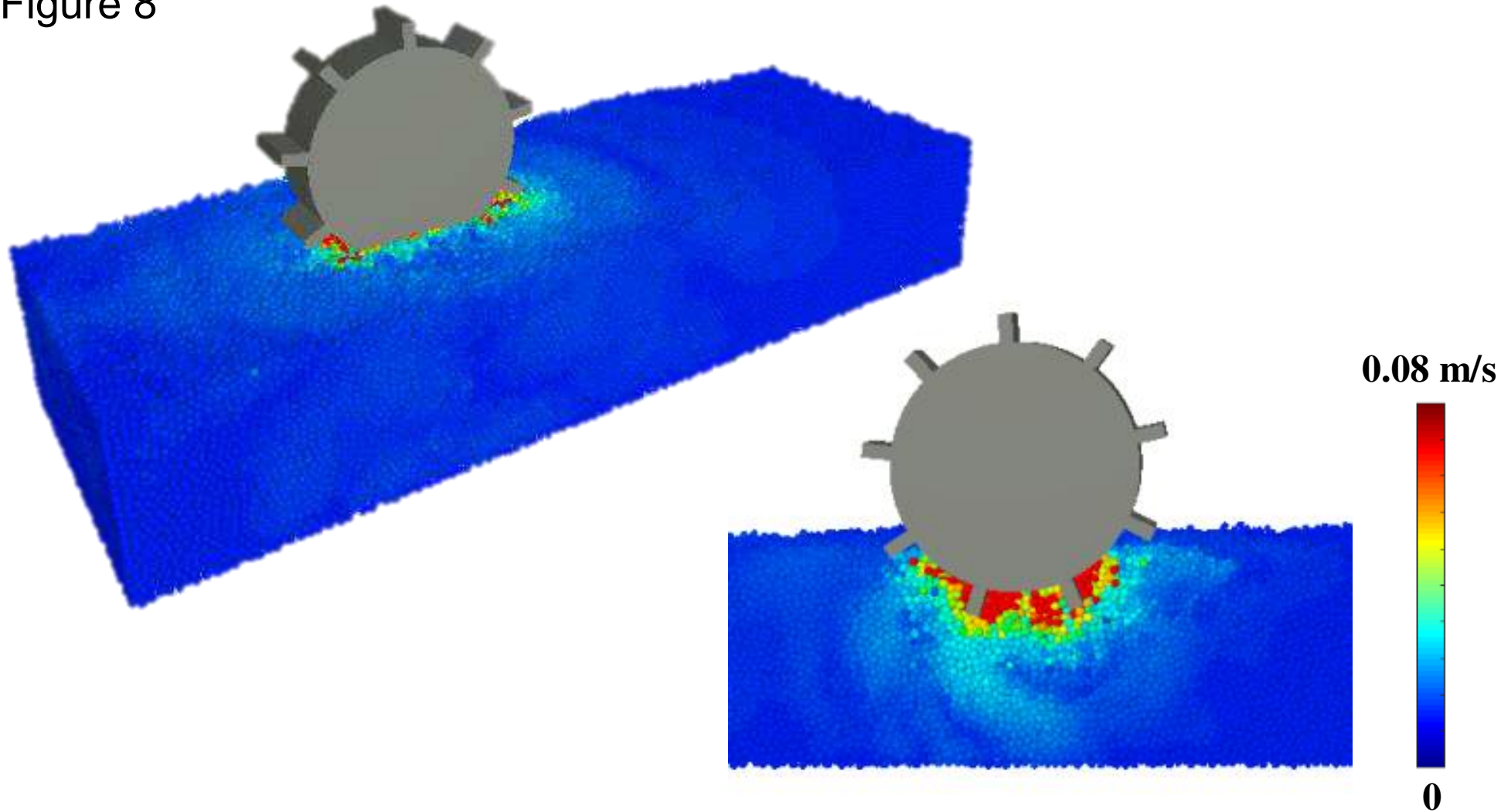

Graphical Abstract (JPEG, PNG or SVG file - 920x300 pixels)

Figures

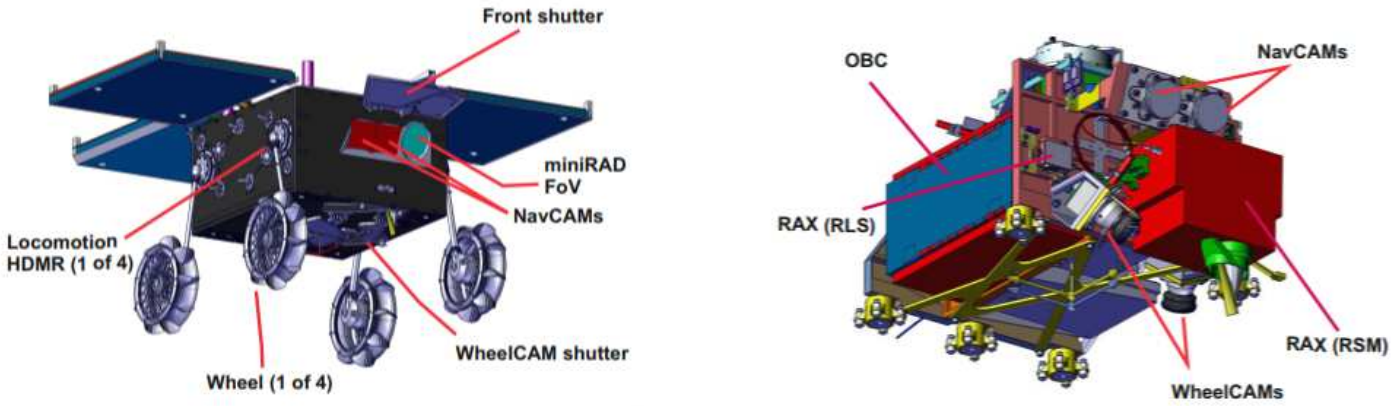

Figure 1

Left: Rover in fully deployed configurations with positions of MiniRad, rear WheelCam and NavCam stereo bench; right: internal compartment (Service Module – SEM) with position if instruments and On Board Computer (OBC). Courtesy from CNES.

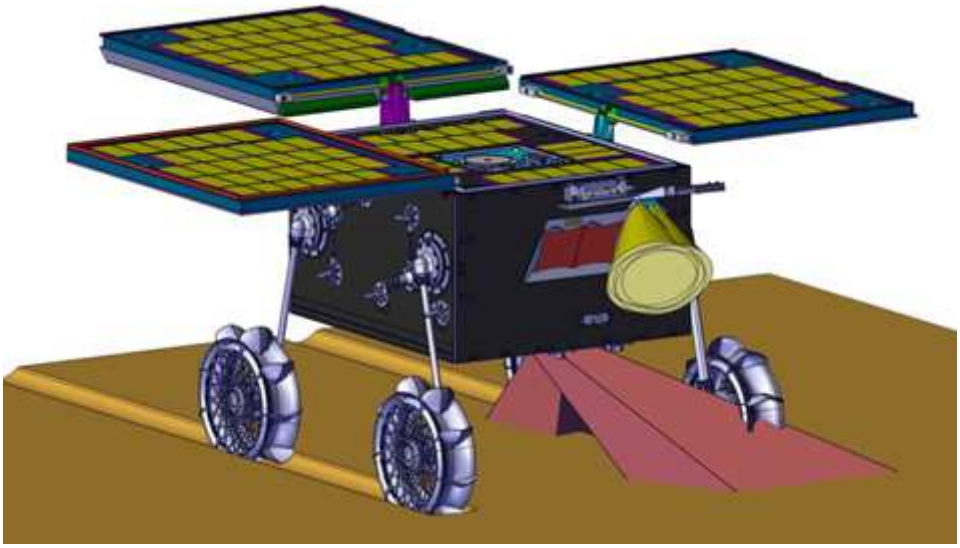

Figure 2

MMX rover with deployed wheels and solar panels in the on-surface configuration. Field of Views of miniRAD and Wheelcams are indicated in yellow and red, respectively. Courtesy from CNES.

Figure 3

CAD model of RAX (Raman spectrometer for MMX).

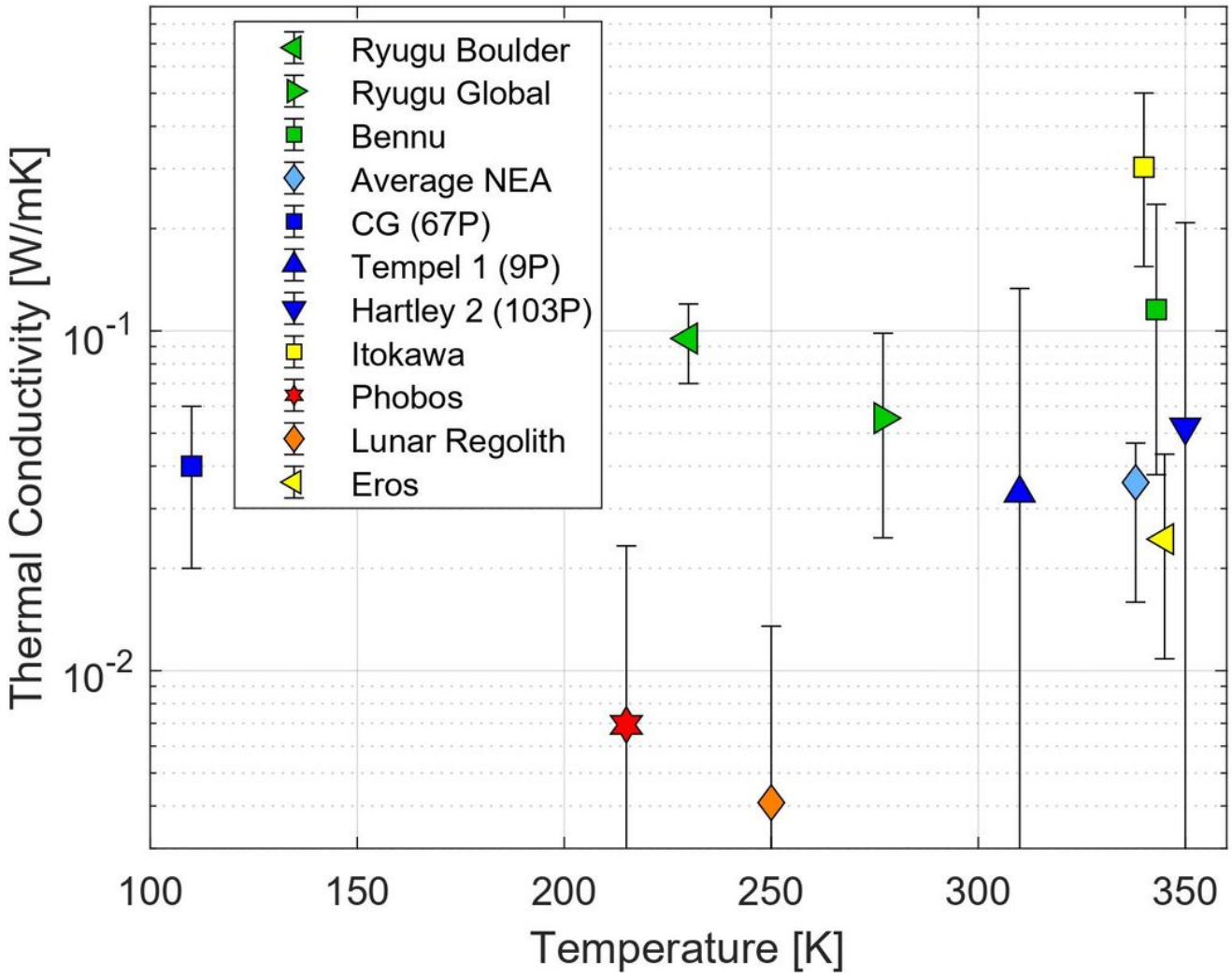

Figure 4

Thermal conductivity as a function of temperature as derived for different small bodies. Data for C-class asteroids Bennu (Emery et al. 2014; Dellagiustina et al. 2019; Rozitis et al. 2019) and Ryugu (Mu¨ller et al. 2017; Hamm et al. 2020), for average near Earth asteroids (Delbo' et al. 2007), for comets 9P/Tempel 1 (Groussin et al. 2013; Davidsson et al. 2009), 103P/Hartley (Groussin et al. 2013), and 67P/Churyumov-Gerasimenko (Spohn et al. 2015), for S-class asteroids Itokawa (Fujiwara et al. 2006) and Eros (Lebofsky and Rieke 1979; Harris and Davies 1999) are shown together with the current best estimate for Phobos (Kuzmin and Zabalueva 2003). For comparison, the thermal conductivity of the lunar regolith (Hayne et al. 2017) is also given.

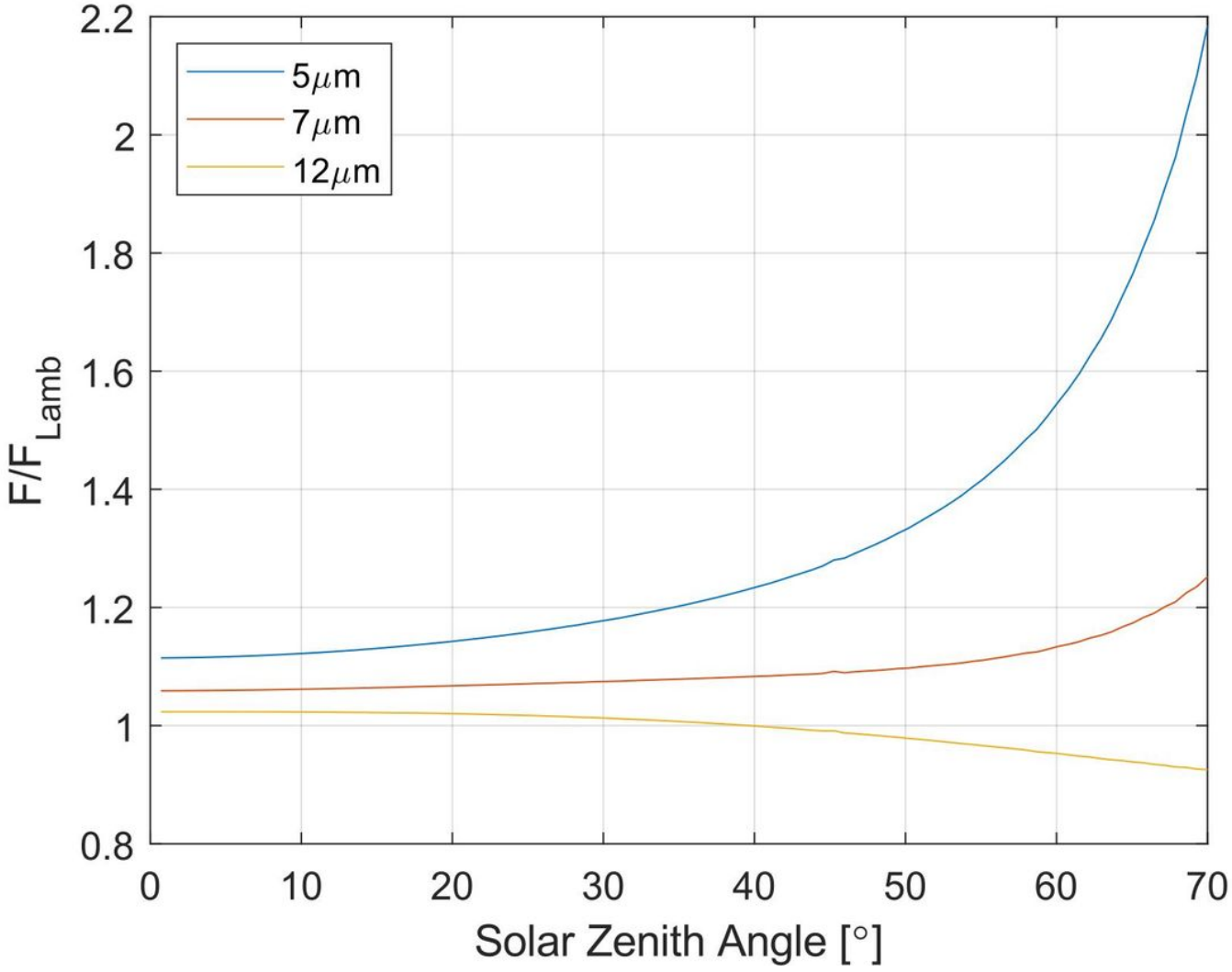

Figure 5

The ratio of flux emitted by a rough surface to that emitted by a flat Lambertian surface as a function of solar zenith angle at three different wavelengths. Results are shown for an equatorial location and a south facing instrument, which observes the surface under an emission angle of 45□.

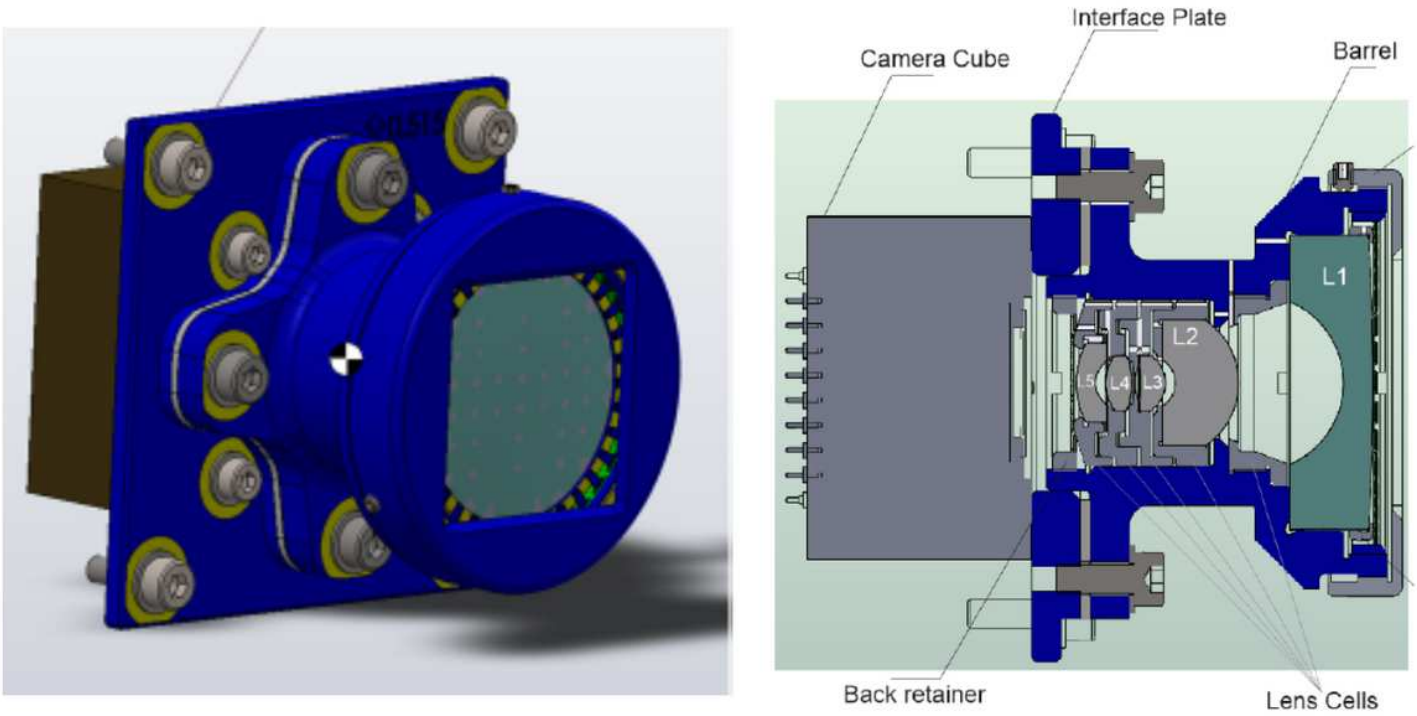

Figure 6

The navigation cameras. Left: CAD view; right: schematic view.

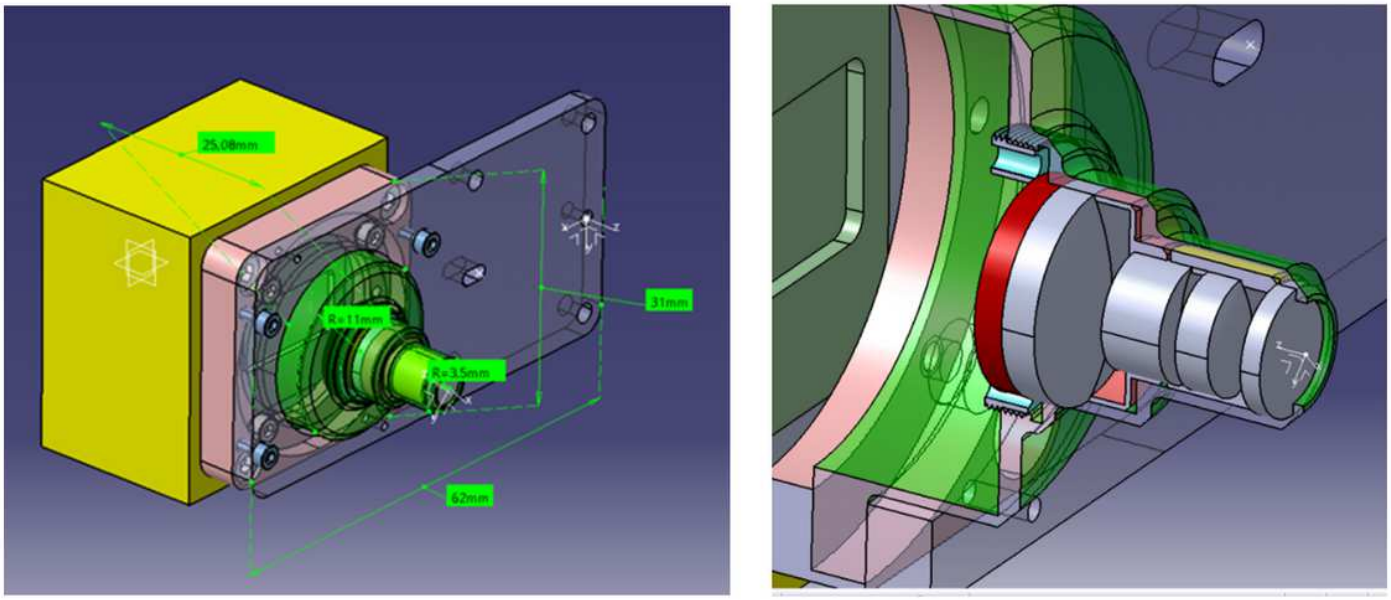

Figure 7

The wheel cameras in their pre-phase A design. Left: CAD view; right: schematic view.

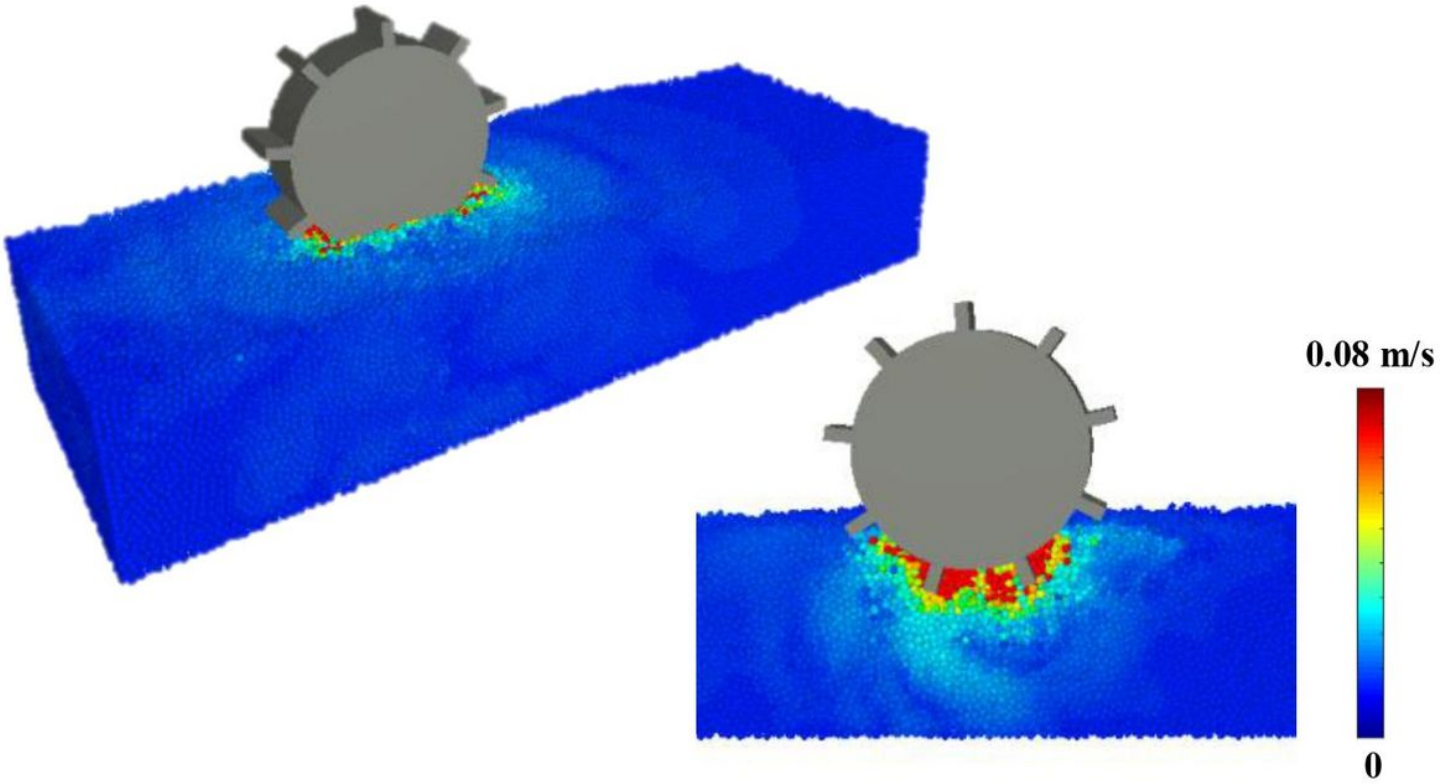

Figure 8

Example SSDEM simulation of a simplified MMX rover wheel traversing a bed of 180,000 cohesionless spherical grains. The wheel is 214 mm in diameter and the grains are 6 ± 0.5 mm in diameter. The simulation was conducted under Earth-gravity using Chrono (Sunday et al. 2020). The grains are colored by velocity magnitude.

Supplementary Files

This is a list of supplementary files associated with this preprint. Click to download.

- RoverPhobos.png